Interfacial Aspects of Adhesion in Polymer Nanocomposite Thin-Film Devices

P. Murugaraj, D. E. Mainwaring, L. G. Chen, P. Sawant, M. Al Kobaisi, W. M. Yek

School of Applied Sciences, Royal Melbourne Institute of Technology, Melbourne 3001, Australia

Received 22 April 2009; accepted 4 July 2009
DOI 10.1002/app.31083
Published online 15 September 2009 in Wiley InterScience (www.interscience.wiley.com).

ABSTRACT: Nanoscale polymeric composites are important in many new electronic technologies, including lightweight and flexible devices and sensors. The influence of surface chemical treatments, which particularly affect the adhesion properties of carbon–polyimide nanocomposite thin films, was studied with infrared spectroscopy, electron microscopy, atomic force microscopy, and contact angle measurements with respect to corresponding polyimide thin films. The contact angles showed that the inclusion of carbon initially increased the hydrophilicity, whereas a potassium hydroxide treatment increased the hydrophilicity of the pure polyimide film and the polyimide component of the nanocomposite surface without increasing the hydrophilicity of the carbon nanoparticle component. Friction-force atomic force microscopy was shown to be a powerful technique for confirming the relative wetting characteristics at the nanoscale. The lower hydrophilicity and activity of the carbon nanoparticles during adhesion reactions reduced the load at break, and this suggests that this conventional modification used for polyimides is less effective for their nanocomposite counterparts. © 2009 Wiley Periodicals, Inc. J Appl Polym Sci 115: 1054–1061, 2010

Key words: adhesion; atomic force microscopy (AFM); nanocomposites; polyimides; thin films

INTRODUCTION

The ability to monitor and control the structural health and usage history of critical infrastructures for both safety and efficiency is increasingly becoming an important aspect of industrial, defense, and national infrastructures. Electrically active polymer thin films are capable of sensing nanoscale strains in both conventional and new lightweight structural materials. Such polymer-based devices also have an added advantage: they can be incorporated within new structural materials such as carbon fiber composites, and this allows these newer materials to be monitored and strain-mapped continuously over their lifetime.

Improvements in the interfacial adhesion of polymers are required not only for the continued advancement of structural sensing devices but also for the development of lightweight and flexible electronic technologies in general as well as improvements in conventional microelectronic fabrication. Certain polyimides (PIs) have been developed to provide superior temperature resistance, mechanical strength, dimensional stability, low dielectric constants, and low dissipation factors. It has been recognized that PIs used in electronic devices often result in poor adhesion and thermal and stiffness mismatches, generating high interfacial stresses that result in displacement, cracking, and delamination issues.[1–3]

Conductive PI nanocomposites, predominately in the form of thin films, are gaining significant prominence, especially in electronics for applications such as electromagnetic interference shielding, electrostatic dissipation, embedded passive components, and positive-coefficient fast-switching devices.[4–8] Nanocomposites have been shown to provide enhanced sensitivities, being capable of sensing nanoscale strains across a range of types of material deformation.[9] These applications require good adhesion and bonding to metallic and nonmetallic substrates for reliable performance.[1,2,8,10] Crosslinked PIs are known to possess weak adhesion characteristics because of their stiff molecular chains, their closed imide rings, and a lack of hydroxyl groups characteristic of effective bonding materials such as cyanoacrylates.[1,2] For both PIs and PI-based composite films, residual stresses due to incorrect adhesion can vary physical properties such as the dielectric constant and electron transport when they are used as active or passive components.

Surface modification by either dry processes or chemical treatments has become the principal route for enhancing the adhesive strength of PI films on various substrates.[8] Physical methods include ion beams, photografting, plasma etching, corona discharge, and sputtering, whereas chemical

Correspondence to: P. Murugaraj (pandiyan.murugaraj@rmit.edu.au).

© 2009 Wiley Periodicals, Inc.

treatments include etching with potassium hydroxide (KOH), ammonium hydroxide, and ethylenediamine;[8,10–15] KOH has become the dominant treatment for PIs. It has been recognized that physical treatments introduce foreign materials into interfaces that may result in reliability failures, whereas chemical-based processes, if well controlled, confine reactions to the surface, resulting in a more homogeneous modification.[12]

Although there are extensive studies on pure PI surfaces, there appear to be no detailed studies on the adhesion of PI nanocomposites onto surfaces employed in electronic device fabrication and utilization. Here we report on the effect of the surface chemical treatment of a carbon nanoparticle/polyimide (C–PI) composite thin film and compare it with its PI counterparts.

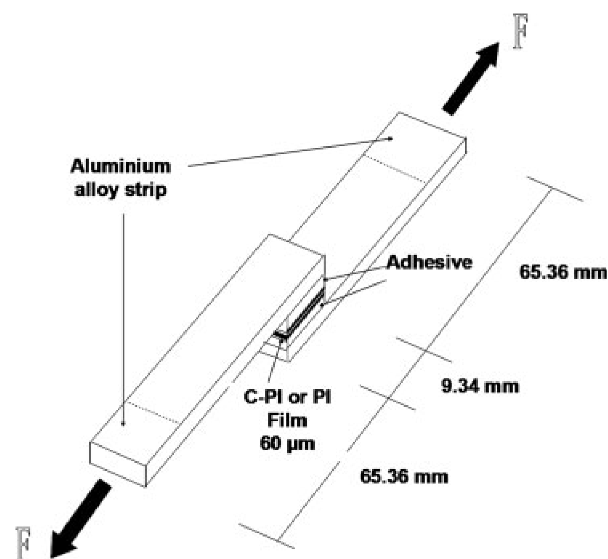

Figure 1 Schematic configuration of a single shear-lap test specimen.

EXPERIMENTAL

Fabrication of the C–PI composite thin films

C–PI composite thin films were fabricated by the thorough dispersion of 30-nm-diameter carbon particles (Vulcan XC72, Cabot Corp., Boston, MA) in a poly(amic acid) mixture of benzophenone tetracarboxylic dianhydride/4,4′-oxybisbenzenamine (BTDA–ODA; HD Microsystems, Parlin, NJ) in *N*-methyl 2-pyrollidone (Sigma–Aldrich Corp., St. Louis, MO) as a solvent by sonication for 1 h (Elma, Singen, Germany) after an *in situ* polymerization process described previously.[16] Freestanding nanocomposite films were produced via slip casting onto glass substrates and subsequent removal with distilled water. All the composite films were soft-baked at 100°C for 10 min and cured at 300°C for 2 h. Slip-cast films had thicknesses in the range of 50–80 μm as determined by profilometry and scanning electron microscopy (SEM) studies. Additionally, Kapton pyromellitic dyanhydride-4,4′-oxidianiline (PMDA–ODA) films (DuPont, Circleville, OH) were also used in this work for comparison.

The KOH treatment was performed on rectangular film sheets (2.0–3.0 cm) and carried out in closed glass flasks. C–PI composite films and Kapton films (PI) were soaked in 0.1, 1.0, and 3.0 mol/L KOH solutions at 25 and 80°C for various times. All samples were cleaned with absolute ethanol before the chemical treatment. After the treatment, these films were removed from the reactive solutions, rinsed in deionized water and then in absolute ethanol, and finally dried at room temperature for 2–3 h.

Characterization

Contact angle measurements between the PI thin-film surface and deionized water was carried out by the sessile drop method (DataPhysics OCA20, DataPhysics Instruments GmbH, Filderstadt, Germany). The static contact angle, advancing contact angle (θ_a), and receding contact angle (θ_r) were measured, and each surface was analyzed with three separate liquid droplets. Fourier transform infrared (FTIR) spectroscopy measurements in the attenuated total reflectance mode (Spectrum 2000, PerkinElmer, Waltham, MA) were carried out with a 45° multiple-reflection zinc selenide attenuated total reflectance crystal element. The scanning range was from 4000 to 700 cm^{-1} with a resolution of 2 cm^{-1} and with 32 scans for each spectrum.

The adhesion strength of the chemically treated C–PI nanocomposite thin films and the corresponding untreated films was evaluated from a single lap-shear test for each sample with aluminum alloy substrates. The bonded-joint aluminum alloy test specimens were fabricated with PI and C–PI films in a sandwich configuration with a cyanoacrylate adhesive (Hottinger Baldwin Messtechnik GmbH, Darmstadt, Germany) in the configuration shown schematically in Figure 1. The sample dimensions followed ASTM D 1002 for the tensile load tests, and the head speed was 1.3 mm/min with the testing temperature maintained at 25°C. The lap-shear strength of the bonded joints was measured with an Instron instrument (Instron 4465, Instron, UK) with a 100-kN transducer.

The surface microstructures were studied with a Quanta 200 environmental scanning electron microscope equipped with an energy-dispersive X-ray analyzer with a Si(Li) X-ray detector (FEI, Hillsboro, OR). Polymer and composite samples were

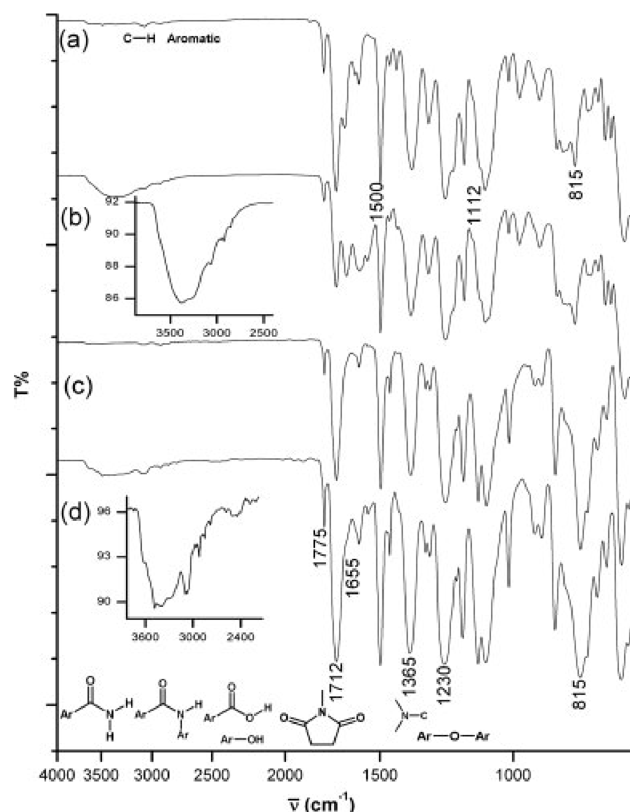

Figure 2 FTIR spectra of (a) the BTDA–ODA PI film before KOH treatment, (b) the BTDA–ODA film after treatment, (c) the Kapton PI (PMDA–ODA) film before treatment, and (d) the Kapton film after treatment. The films were treated with 0.1*M* KOH for 30 min at 80°C.

sputtered with a nanometer gold layer to provide charge dissipation within the beam of the environmental scanning electron microscope.

Atomic force microscopy (AFM) studies were carried out on a NanoScope IIIa multimode AFM instrument (Veeco Instruments, Inc., New York, NY) in the tapping, contact, and friction-force modes at room temperature and a relative humidity of 40%. Commercially available Si_3N_4 tips on 100-μm triangular cantilevers (spring constant = 0.58 N/m) were used to measure the friction-force behavior of polymeric nanocomposite surfaces in the contact mode. The spring constant and the frequency of tapping-mode phosphorus-doped silicon cantilevers were 40 N/m and 300 kHz, respectively. Friction at the nanoscale was measured by the simultaneous measurement of the vertical (normal) force (F_{normal}) and the average lateral force ($F_{lateral}$) acting on the surface by the tip. The coefficient of friction (M) is thus given by the following expression:

$$M = \langle |F_{lateral}| \rangle / F_{normal}$$

Capillary forces play an important role in the contact and friction-force analysis because tips with dimensions less than 10 nm act as nuclei for the condensation of water vapor in air. These forces give rise to a water meniscus between the tip and the substrate, and therefore large forces are required to bring the tip into contact with the hydrophilic surface. Capillary forces are short-range forces and have an impact on a large part of the tip. Therefore, such capillary forces can be used to differentiate at the nanoscale between hydrophobic and hydrophilic regions during friction-force microscopic analysis, and thus spatial chemical heterogeneity on the surface at the nanoscale can be identified.[17–19]

RESULTS AND DISCUSSION

FTIR analysis

Figure 2 shows the FTIR spectra of the BTDA–ODA PI and PMDA–ODA PI (Kapton) films in both the initially untreated and chemically treated states, whereas Figure 3 shows the corresponding C–PI (BTDA–ODA) spectra. In the untreated films [Figs. 2(a,c) and 3(a)], absorption bands in the spectra can be assigned to the principal PI functional groups as reported previously,[20–22] with only small variations. PI is characterized by C=O symmetric and asymmetric stretching of the imide ring at 1775 and 1712 cm^{-1}, a *p*-phenylene stretching band at 1500 cm^{-1}, deformation bands at 1112 and 815 cm^{-1}, C—N stretching of the pyromellitic imide system band at 1365 cm^{-1}, and an aromatic ether stretching band at 1230 cm^{-1}.

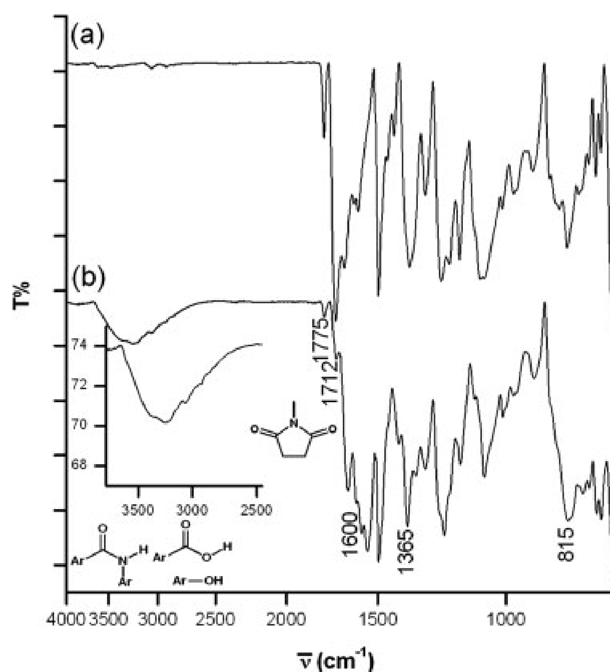

Figure 3 FTIR spectra of the C–PI (BTDA–ODA PI) nanocomposite film (a) before KOH treatment and (b) after treatment with 0.1*M* KOH for 30 min at 80°C.

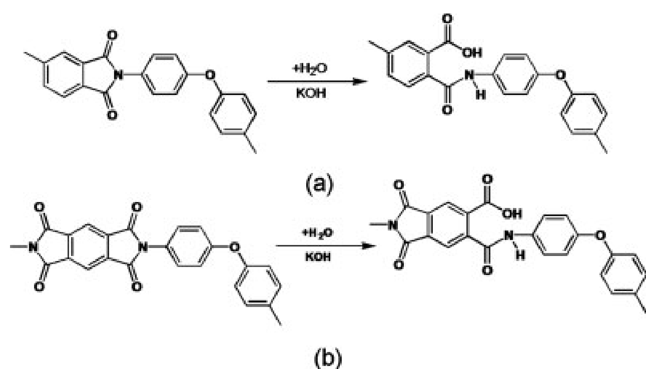

Figure 4 Structural changes in (a) the BTDA–ODA PI and (b) the PMDA–ODA PI due to hydrolysis with KOH.

After treatment with 0.1*M* KOH at 80°C for 30 min, both the PI and C–PI films exhibited changes in the absorption spectra. The intensity of the C=O band of the imide ring at 1775 and 1712 cm^{-1} decreased for both PI and C–PI films to different degrees. Broad bands between 3600 and 2800 cm^{-1} appeared because of the formation of carboxylic acid and amide groups in the PI films [Fig. 2(b,d)] and in the C–PI nanocomposite film [Fig. 3(b)]. The pyromellitic imide (C—N) band at 1365 cm^{-1} decreased continuously, and this was indicative of severe cleavage of the imide ring. The strong reduction in the aromatic ether stretching band at 1230 cm^{-1} demonstrated the cleavage of the ether bond as well the formation of phenolic OH groups.

For both the PI and C–PI films, bands at 1400 and 1600 cm^{-1} appeared as shoulders to the dominant bands at 1598 and 1365 cm^{-1} when they were treated with KOH; this may have been due to the salt form of the carboxylic and amide groups, which would be consistent with Okumura et al.[22] Figures 2(a,c) and 3(a) indicate that a very small 1600-cm^{-1} band existed for the untreated films because of the aromatic ring,[23] which may also have contributed to the spectrum of the treated films. Additionally, the out-of-plane deformation band observed at 815 cm^{-1} became broader and weaker because of the formation of a multisubstituted benzene ring.[22] Kim et al.[24] assigned the characteristic band at 1655 cm^{-1} to the amide carbonyl stretching in the PI film before curing and annealing, as shown in Figure 2(b,d), but it was masked in the broader peaks of C–PI [Fig. 3(b)]. The appearance of this peak after KOH confirmed the opening of the imide ring to form poly(amic acid) on the surface of the treated PI film, as illustrated in Figure 4(a,b) for both the PMDA–ODA and BTDA–ODA molecular structures.

Surface microstructure

To further characterize these changes, the surface microstructure was examined with environmental scanning electron microscopy (ESEM). Figure 5 shows the development of physical surface features with the increasing severity of the chemical treatment. Figure 5(a) shows the featureless surface of the untreated C–PI nanocomposite, whereas Figure 5(b) shows the development of elongated surface trenches with the treatment time; the insets show

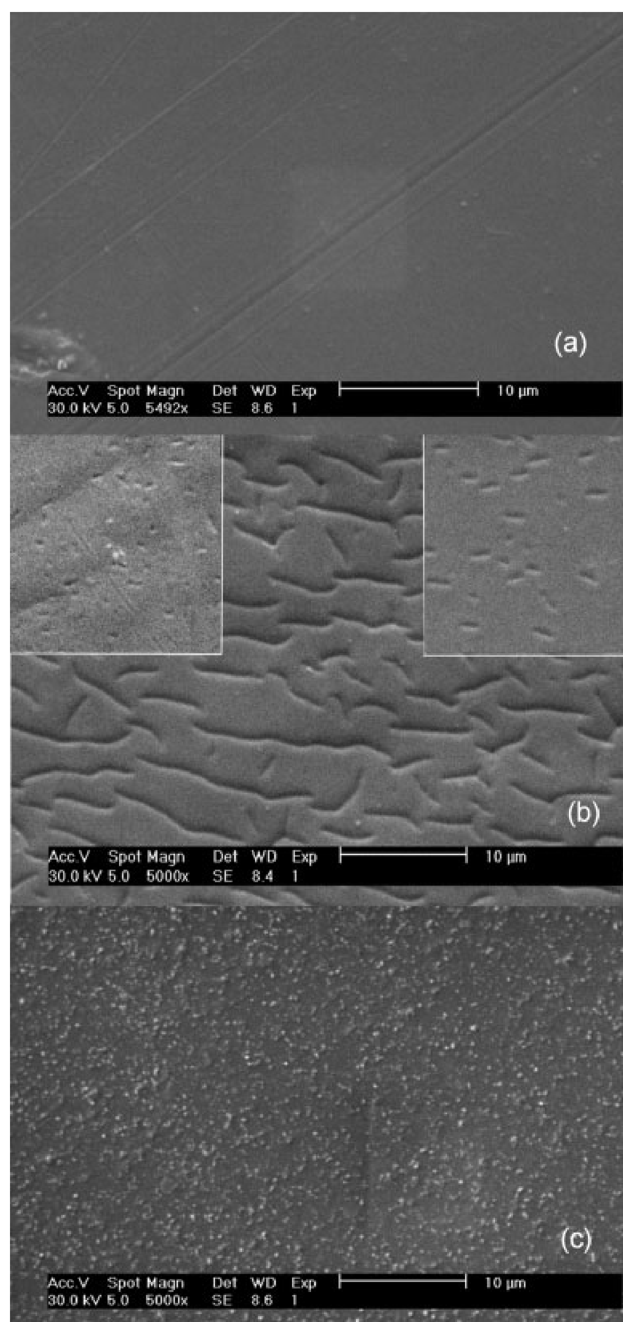

Figure 5 SEM images of (a) the untreated C–PI nanocomposite film surface, (b) the C–PI nanocomposite treated with 0.1*M* KOH at 80°C for 30 min, and (c) the C–PI nanocomposite film surface treated with 3.0*M* KOH at 25°C for 9 min. In part B, the inset on the left shows C–PI treated with 0.1*M* KOH at 80°C for 1 min, and the inset on the right shows the C–PI film surface-treated for 50 min.

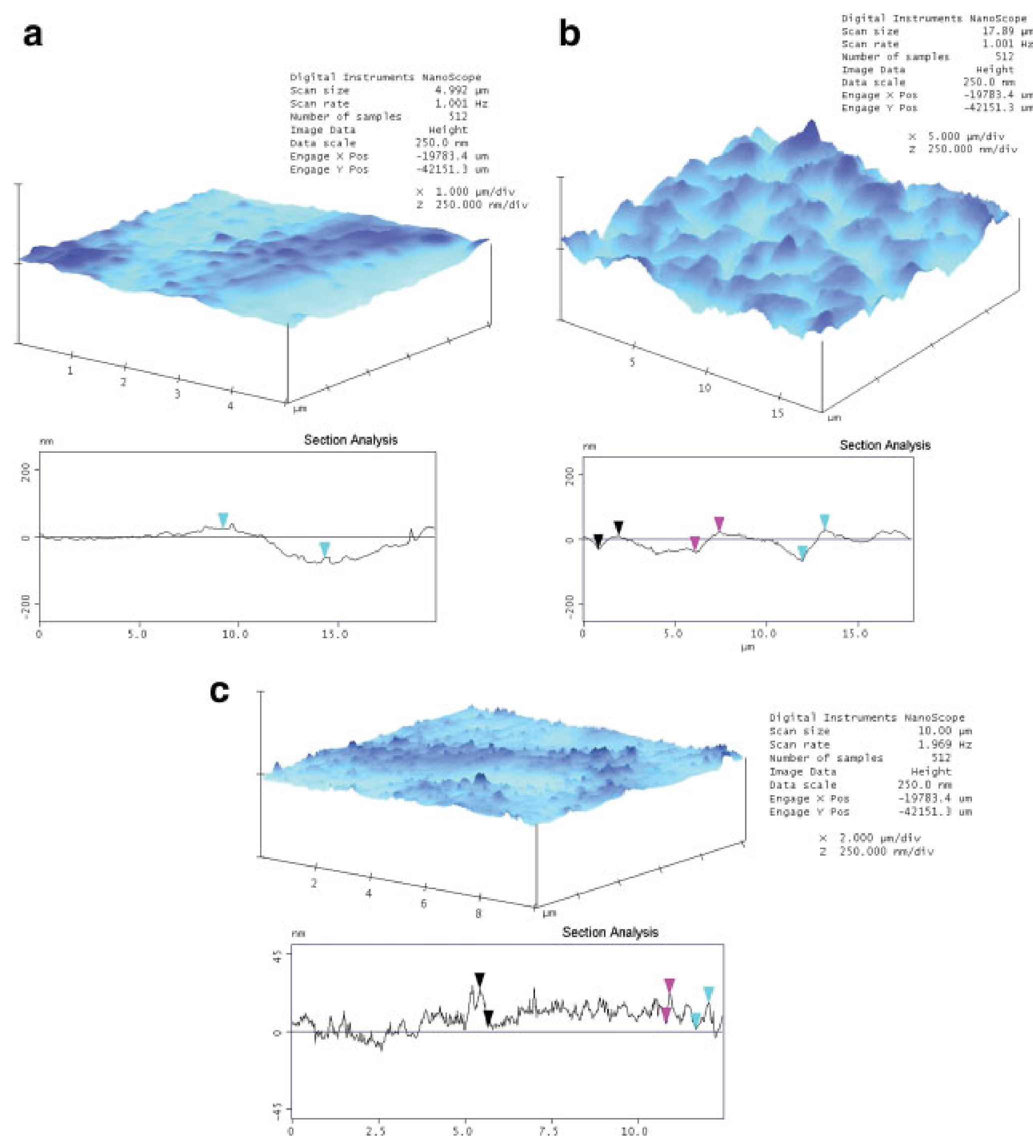

Figure 6 Three-dimensional height scan images of (a) the C–PI nanocomposite surface before the chemical treatment, (b) the C–PI nanocomposite surface after treatment with 0.1*M* KOH at 80°C for 30 min, and (c) the C–PI nanocomposite surface after treatment with 3.0*M* KOH at 25°C for 9 min. [Color figure can be viewed in the online issue, which is available at www.interscience.wiley.com.]

their initiation as etched pits at 1 min and their ultimate erosion after prolonged treatment times (50 min). A severe surface treatment (e.g., 3*M* KOH) partially eroded the whole nanocomposite surface, leaving exposed protruding carbon nanoparticle clusters, as shown in Figure 5(c).

The submicrometer surface topology plays an important role in the surface wetting and adhesion of polymer thin films. AFM was employed to monitor these microstructural changes introduced onto the C–PI nanocomposite thin film surfaces through the KOH treatment. Figure 6(a) shows the three-dimensional height scan image obtained in the tapping mode for an untreated C–PI nanocomposite thin film. The film surface contained undulating features originating from film fabrication processes and localized spherical features attributable to carbon clusters within the film matrix; this resulted in an initial film surface that was otherwise smooth [see the sectional analysis in Fig. 6(a)]. Roughness analysis of the smooth area yielded an average roughness value of 2.687 nm and a root mean square value of 3.466 nm.

Height scans on the surfaces that showed the presence of elongated trenches with the KOH treatment [Fig. 5(b)] confirmed the formation of this trenchlike morphology [Fig. 6(b)]. Here the roughness analysis yielded an average roughness value of 18.931 nm and a root mean square value of 23.952 nm, which confirmed the development of significant indentations at depths of about 50 nm, which may be able to enhance the surface engagement of adhesive phases, and showed limited sharp protrusions

indicative of exposed carbon clusters. An AFM examination of the severely treated composite surfaces [Fig. 6(c)] showed increased sharp protrusions distinctly different from the topological features observed in both previous samples [Fig. 6(a,b)]. Here the average roughness declined to 6.386 nm, and the root mean square declined to 8.068 nm; this confirmed the partial dissolution of the film surface and the prevalence of exposed nanoscale carbon clusters.

Surface wetting

Information on the processes influencing surface wetting and adhesion can be gained from both θ_a and θ_r and the differences between them (i.e., contact angle hysteresis).[25,26] Equilibrium contact angles, different from a single unique value, may be due to inhomogeneous compositions and rough surface features as well as specific molecular interactions occurring at this interface.[27,28] θ_a and θ_r measurements were carried out for the nanocomposite C–PI and PI films with samples treated with three concentrations of KOH for various times at 80°C and for the respective untreated films (Fig. 7). Figure 7(a) shows θ_a and θ_r of the PI and C–PI films and those treated with KOH for 10 and 30 min; before the KOH treatment, both θ_a and θ_r were lower for the C–PI film than for the PI film because of the carbon inclusions providing areas of greater hydrophilicity and roughness. The KOH treatment increased the hydrophilicity of both the PI and C–PI films, as shown by the decline of θ_a and θ_r with the KOH concentration. The constant hysteresis ($\theta_a - \theta_r$) with the KOH concentration increasing up to 1*M* showed that this surface treatment produced a constant surface roughness. Figure 7(b) indicates that the surface roughness remained constant for various treatment times at these low KOH concentrations. At higher KOH concentrations (3*M* KOH), the wetting behavior was quite different [Fig. 7(c)]. Here, for the PI polymer film treated for 9 min, the surface roughness and heterogeneity disappeared, as indicated by $\theta_a = \theta_r$, whereas the C–PI nanocomposite film remained constant with respect to roughness because of carbon inclusions, and the hydrophilicity continued to decrease, as shown by the slopes of the curves. This wetting behavior, together with the lower overall θ_a and θ_r values of both PI and C–PI, indicated that the surface roughness of the PI film decreased with erosion at a KOH concentration of 3*M*, whereas the C–PI film roughness was constant because of exposed carbon nanoparticles; however, the surface hydrophilicity of the C–PI film remained constant with the KOH treatment, although it increased significantly in the PI film and in the PI component of the C–PI film. These microstructural changes were

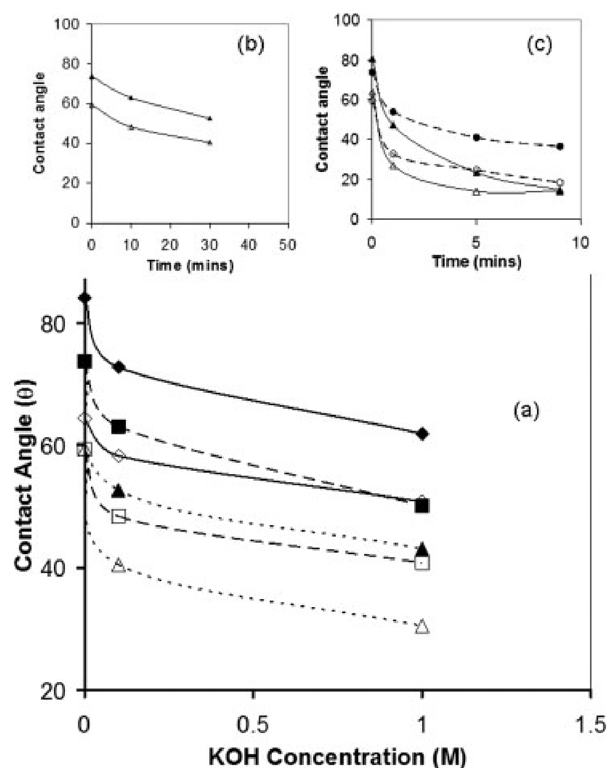

Figure 7 θ_a (closed symbols) and θ_r (open symbols) on (a) (◆) PI and (■,▲) C–PI films treated with KOH at 80°C [PI was treated for 10 min, and C–PI was treated for (■) 10 or (▲) 30 min], (b) C–PI films treated with 0.1*M* KOH with time, and (c) (▲) PI and (●) C–PI films treated with 3.0*M* KOH with time.

consistent with the ESEM data [Fig. 5(c)] and the AFM data [Fig. 6(c)].

Adhesion strength

Figure 8 shows the load–displacement curves obtained from single shear-lap tests performed on treated and untreated C–PI composite and corresponding PI films. The load at break for the untreated C–PI nanocomposite thin film was 305 N, which corresponded to an applied stress of 480.6 MPa. After the chemical treatment of the C–PI film with 0.1*M* KOH at 80°C for 30 min [Fig. 8(a)], the load at break increased by 12% to 345 N (applied stress = 563.9 MPa). A similar evaluation of the PI films before the chemical treatment gave a load at break value of 404 N (applied stress = 668.0 MPa) slightly greater than that of the untreated composite thin film. After a similar KOH treatment, the load at break value of the PI film increased by 108% to 842 N (applied stress = 1376 MPa). Thus, although the films exhibited similar adhesive strengths before the chemical treatment, the reduction in the degree of enhancement of the nanocomposite film is indicative of the emergence of significant differences in the

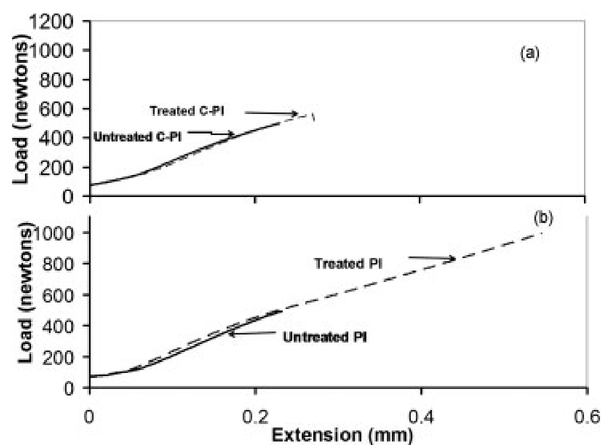

Figure 8 Applied load versus extension during single shear-lap testing of PI (BTDA–ODA) and C–PI films: (a) the initial C–PI film and the C–PI film treated with 0.1*M* KOH at 80°C for 30 min and (b) the initial PI film and the film after similar KOH treatment.

surface structural and chemical effects and indicates that conventional surface modification techniques are not applicable to these types of nanocomposite polymer thin films.

Friction-force microscopy

To further understand these differences in surface treatment, the emergence of surface OH groups identified in FTIR measurements (Fig. 2) was evaluated spatially by friction-force measurements with the AFM system, by which topographic and friction images could be obtained simultaneously. AFM height scans performed in the tapping mode on severely treated nanocomposite thin film surfaces [Fig. 6(c)] clearly showed exposed carbon nanoclusters that were consistent with the ESEM image [Fig. 5(c)]. Friction-force images of the same area provided information on the wetting characteristics of this surface. Figure 9 shows the three-dimensional image of the lateral-force scan obtained for this sample; the frictional forces were found to be less over the exposed carbon nanoparticles in comparison with those on the surrounding PI surface. Because the contact-mode AFM tip was hydrophilic Si_3N_4,[17–19] the tip generated a stronger friction force on the more hydrophilic area, that is, the treated PI, than on the exposed carbon area.

The identification by friction-force AFM of areas of the treated PI surface that were more hydrophilic than the corresponding carbon cluster inclusion areas is consistent with the macroscopic-scale contact angle measurements, by which it could be clearly seen that both θ_a and θ_r decreased with the inclusion of carbon in the surfaces, and this lowering continued with increasing KOH treatment [Fig. 7(a)]. As the PI polymer film was treated with KOH for longer times, its hydrophilicity increased at a greater rate than that of the corresponding C–PI nanocomposite film. This could be clearly seen in the θ_a curves converging at 9 min despite different initial values [Fig. 7(c)]. The adhesion lap tests (Fig. 8) also indicated that the KOH treatment enhanced the load at break more in the PI films than in the corresponding C–PI nanocomposite films.

CONCLUSIONS

In this study, we investigated differences in surface treatments affecting the adhesion of PI thin films and their corresponding carbon nanocomposite films. FTIR studies showed that the conventional KOH treatment used to enhance surface wetting and adhesion in the electronics industry produced an opening of the imide rings to form surface poly(amic acid) as well as other carboxylic acids and amide groups. ESEM and AFM studies showed the evolution of microstructural features responsible for surface roughness, which included etch pits and elongated surface trenches and finally a smooth, eroded polymer surface, whereas the exposed inclusions in the nanocomposite remained constant.

Before the KOH treatment, the presence of carbon nanoparticle inclusions lowered the contact angle; this indicated that initially carbon was a more hydrophilic surface. With increasing KOH treatment, the contact angle hysteresis ($\theta_a - \theta_r$) showed that the surface treatment increased the roughness of the PI film and the PI component of the nanocomposite component at first, but this was reduced by erosion at high KOH concentrations. Although carbon

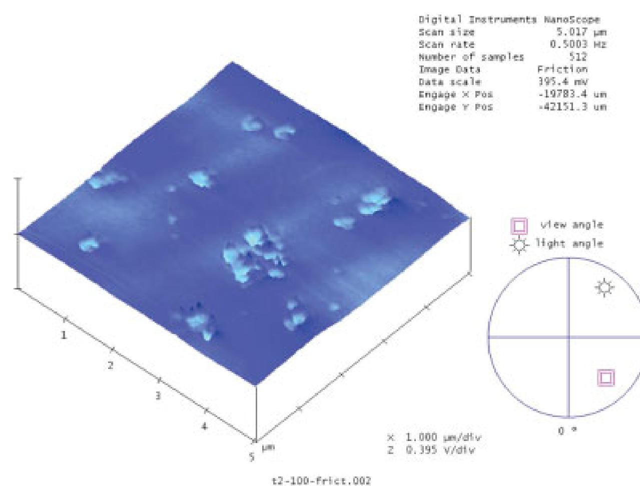

Figure 9 Three-dimensional friction-force image of the C–PI nanocomposite surface after a severe chemical treatment (3.0*M* KOH at 25°C for 9 min). [Color figure can be viewed in the online issue, which is available at www.interscience.wiley.com.]

nanoparticles in untreated films initially increased their hydrophilicity, the KOH treatment increased the hydrophilicity of the PI component but not that of the carbon nanoparticles themselves. Tensile tests showed that although the increase in the load at break was considerably higher for the PI films after the surface treatment, the corresponding C–PI films exhibited only minor enhancements. Friction-force AFM microscopy of the KOH-treated C–PI indicated that the exposed carbon nanoparticle surfaces were less hydrophilic than the surrounding PI surface component. This independently confirmed that although the inclusion of carbon nanoparticles in the PI film initially increased the hydrophilicity of the film, progressively increasing the KOH treatment functionalized the PI surface to a greater extent than the exposed carbon nanoparticle component. This resulted in the nanocomposite surfaces being less hydrophilic than the corresponding PI and the nanoparticle surfaces being less active than PI in reactions with the adhesive, producing lower adhesion strengths. This suggests that the conventional surface modification used for PI films is less effective for their heterogeneous nanocomposite counterparts.

References

1. Ree, M.; Chu, C.-W.; Goldberg, M. J. J Appl Phys 1994, 75, 1410.
2. Ree, M.; Chen, K.-J.; Kirby, D. P.; Katzenellenbogen, N.; Grischikowsky, D. J Appl Phys 1992, 72, 2014.
3. Ho, P. S. Appl Surf Sci 1989, 41, 559.
4. Luo, S.; Wong, C. P. IEEE Trans Comput Packaging Technol 2000, 23, 151.
5. Nakamura, S.; Tomimura, T. IEE Conf Publ 2000, 473, 265.
6. Strumpler, R.; Glatz-Reichenbach, J. J Electroceram 1999, 3, 329.
7. Jagur-Grodzinski, J. Polym Adv Technol 2002, 13, 615.
8. Ranucci, E.; Sandgren, A.; Andronova, N.; Albertsson, A.-C. J Appl Polym Sci 2001, 82, 1971.
9. Mainwaring, D.; Murugaraj, D.; Mora-Huertas, N.; Sethupathi, K. Appl Phys Lett 2008, 92, 253303.
10. Lee, S.; Park, S. S.; Lee, H. K. Macromol Symp 2007, 249, 586.
11. Vasquez, D. L.; Ndalama, T.; Hirschfeld, D. A. High Perform Polym 2005, 17, 293.
12. Park, S.-J.; Lee, E.-J.; Kwon, S.-H. Bull Korean Chem Soc 2007, 28, 188.
13. Lin, Y.-S.; Liu, H.-M.; Tsai, C.-W. J Polym Sci Part B: Polym Phys 2005, 43, 2023.
14. Kim, S.-H.; Cho, S. H.; Lee, N.-E.; Kim, H. M.; Nam, Y. W.; Kim, Y.-H. Surf Coat Technol 2005, 193, 101.
15. Butoi, C. I.; Steen, M. L.; Peers, J. R. D.; Fisher, E. R. J Phys Chem 2001, 105, 5957.
16. Murugaraj, P.; Mora-Huertas, N.; Mainwaring, D. E.; Ding, Y.; Agrawal, S. Compos A 2008, 39, 308.
17. Nicolau, D. V.; Sawant, P. D. Top Curr Chem 2005, 260, 113.
18. Noy, A.; Frisbie, C. D.; Rozsnyaim, L. F.; Wrighton, M. S.; Lieber, C. M. J Am Chem Soc 1995, 117, 7943.
19. Sirghi, L.; Aoki, T.; Hatanaka, Y. Thin Solid Films 2002, 422, 55.
20. Choukourov, A.; Hanus, J.; Kousal, J.; Grinevich, A.; Pihosh, Y.; Slavinska, D.; Biederman, H. Vacuum 2006, 80, 923.
21. Hummel, D. O.; Goettgens, S.; Neuhoff, U.; Duessel, H. J. J Anal Appl Pyrolysis 1995, 33, 195.
22. Okumura, H.; Takahagi, T.; Nagai, N.; Shingubara, S. J Polym Sci Part B: Polym Phys 2003, 41, 2071.
23. Snyder, R. W.; Thomson, B.; Bartges, B.; Czerniawski, D.; Painter, C. Macromolecules 1989, 22, 4186.
24. Kim, S. H.; Lee, D. W.; Chung, K.-H.; Park, J. K.; Jaung, J.-Y.; Jeong, S. H. J Appl Polym Sci 2002, 86, 812.
25. Good, R. J.; Koo, M. N. J Colloid Interface Sci 1979, 71, 283.
26. Cain, J. B.; Francis, D. W.; Venter, R. D.; Neumann, A. W. J Colloid Interface Sci 1983, 94, 123.
27. Marmur, A. Adv Colloid Interface Sci 1994, 50, 121.
28. Wu, S. Polymer Interface and Adhesion; Marcel Dekker: New York, 1982.